THE JOURNAL OF PHYSICAL CHEMISTRY Letters

Letter

pubs.acs.org/JPCL

Salt Pumping by Voltage-Gated Nanochannels

Mario Tagliazucchi[†,‡] and Igal Szleifer*[,†]

[†]Department of Biomedical Engineering, Department of Chemistry and Chemistry of Life Processes Institute, Northwestern University, Evanston, Illinois 60208, United States

[‡]INQUIMAE-CONICET, Ciudad Universitaria, Pabellón 2, Ciudad Autónoma de Buenos Aires C1428EHA, Argentina

Supporting Information

ABSTRACT: This Letter investigates voltage-gated nanochannels, where both the potential applied to the conductive membrane containing the channel (membrane potential) and the potential difference between the solutions at both sides of the membrane (transmembrane potential) are independently controlled. The predicted conductance characteristics of these fixed-potential channels dramatically differ from those of the widely studied fixed-charge nanochannels, in which the membrane is insulating and has a fixed surface charge density. The difference arises because the transmembrane potential induces an inhomogeneous charge distribution on the surface of fixed-potential nanochannels. This behavior, related to bipolar electrochemistry, has some interesting and unexpected consequences for ion transport. For example, continuously oscillating the transmembrane potential, while holding the membrane potential at the potential for which it has zero charge in equilibrium, creates fluxes of neutral salt (fluxes of anions and cations in the same direction and number) through the channel, which is an interesting phenomenon for desalination applications.

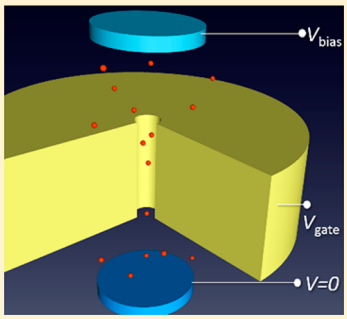

The outstanding transport properties of biological channels have inspired researchers to create and study synthetic channels and pores mimicking some of their functional aspects, such as response to stimuli.[1,2] Among the different stimuli used to externally tune the conductance of synthetic channels,[1−3] membrane potential is unique because it provides a direct, continuously tunable and fast-operating handle over charge selectivity.[4−16] Martin and collaborators[5−8] and Hinds and collaborators[9,10] reported nanochannels where the selectivity toward concentration-driven transport was switched between anionic and cationic by the potential applied to the membrane.

Recently, Martin[11] and Albrecht[12] groups reported potential-driven transport through voltage-gated nanochannels, where both the transmembrane and the membrane potentials are simultaneously controlled using a bipotentiostat. This experiment allows electrically driving the translocation of charged molecules through the pore, while simultaneously gating and tuning selectivity with the membrane potential. Theoretical work in the literature have extensively addressed fixed-charged insulating membranes, but very few works addressed the theory of these fixed-potential nanochannels.[14,15] In this work, we present theoretical studies of the conductance properties of fixed-potential nanochannels and show that they are qualitatively different from those of fixed-charge channels. The differences between fixed-charge and fixed-potential nanochannels are important for applications: we demonstrate here the pumping of neutral salt (i.e., pumping of anions and cations in the same direction and number) by oscillation of the transmembrane potential in voltage-gated nanochannels.

Figures 1a and 1b show schemes of nanochannels with a fixed charge density (fixed-charge channel) and voltage-gated nanochannels (fixed-potential channel), respectively. In the fixed-potential case, the membrane potential is V_{gate}. In both cases, the potential bias for the electrode located at the upper reservoir is V_{bias} and the potential for the electrode located at the lower reservoir is zero by convention (i.e., choice of zero of the electrostatic potential), see Figure 1. Note that in an experimental realization using a bipotentiostat,[11] the lower reservoir will contain the reference and counter electrodes and the electrode in the upper reservoir and the membrane will be working electrodes. Experimentally, the membrane potential, V_{gate}, is measured with respect to a reference electrode[11,12] (the transmembrane potential is independent of the reference electrode when the reference electrode and the working electrode in the upper reservoir are of the same type, i.e. Ag/AgCl). For simplicity, we report V_{gate} with respect to the potential at which the metal has zero charge (potential of zero charge of the metal),[17] i.e. in the absence of a transmembrane potential, the charge of the membrane is zero for V_{gate} = 0 V. This choice of reference allows qualitative comparison with experiments using gold membranes and Ag/AgCl reference electrodes, because the potential of zero charge of gold is only 40−100 mV more positive than the Ag/AgCl reference potential.[18] In experiments, Faradaic currents due to the oxidation of the solvent or the electrode or reduction of oxygen may occur for large absolute values of V_{gate} and V_{bias}. Therefore, we decided to limit our potential range from −1 to 1 V for both V_{gate} and V_{bias} based on experiments in the literature.[11]

We studied the systems in Figures 1a and 1b, by solving the Poisson-Nernst-Planck-Navier-Stokes (PNP-NS) system of

Received: June 20, 2015
Accepted: August 25, 2015

DOI: 10.1021/acs.jpclett.5b01315
J. Phys. Chem. Lett. 2015, 6, 3534−3539

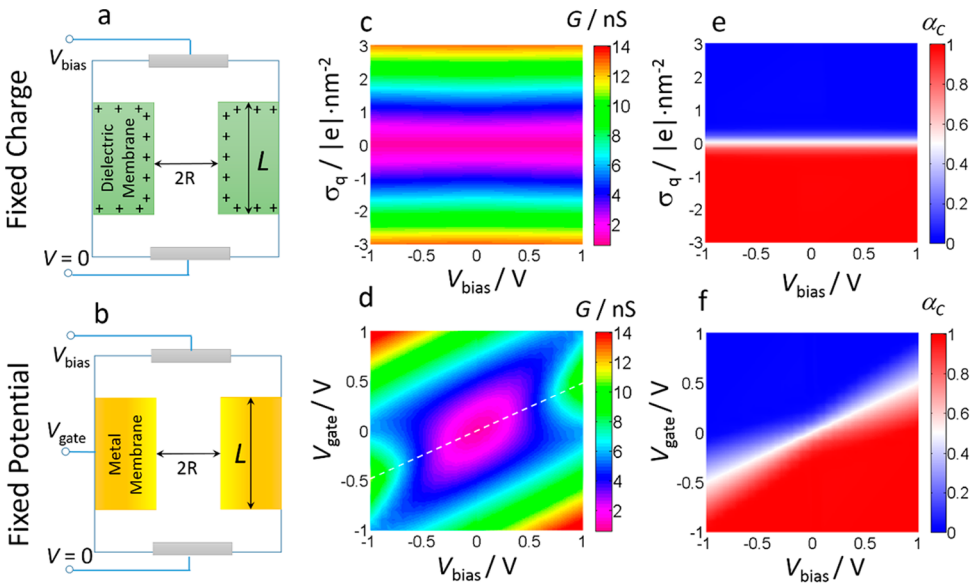

Figure 1. a, b. Schemes of the systems under study. A single nanochannel of length L and radius R in a membrane connects two reservoirs. Each reservoir contains an electrolyte solution, composed of water molecules, cations and anions, and a reversible electrode. The membrane may be either insulating with a fixed surface charge density σ_q (fixed-charge system, panel a) or conducting with a constant potential V_{gate} (fixed-potential system, panel b). The potential of the electrode in the lower reservoir is $V = 0$ by convention and the potential of the electrode in the upper reservoir is V_{bias}. **c, d.** Color maps of the conductance ($G = I/V_{bias}$) as a function of V_{bias} and σ_q for the fixed-charge system (panel c) or as a function of V_{bias} and V_{gate} for the fixed-potential system (panel d) for a nanochannel of L = 250 nm and R = 7.5 nm and a bulk salt concentration of 0.1 M. The white dashed line in panel *d* shows $V_{gate} = V_{bias}/2$. **e, f.** Color maps of the cationic selectivity, defined as $\alpha_C = |G_C|/G$ (where G_C and G are the conductance due to the cations and the total conductance, respectively) for the same conditions as in panels **c** and **d**.

coupled equations.[19] This continuum model is valid for channel radii larger than two Debye lengths (R > 2 nm for a 0.1 M solution).[20] We modeled the electrode/solution interface using the Gouy−Chapman-Stern (GCS) model,[21] which is the simplest model that captures the capacitance properties of bare metal electrodes. The GCS model considers the finite size of the ions by limiting their distance of maximum approach to the electrode surface; the region inaccessible to the ions is known as the Stern layer. We present a detailed description of our theoretical methodology in the Supporting Information.

Figures 1c and 1d show color maps of the steady-state conductance, $G = I/V_{bias}$ for the fixed-charge and fixed-potential channels, respectively. The predicted conductance, described in detail in previous publications,[22−27] is independent of V_{bias}, which indicates a linear (ohmic) I-V response, and it has a minimum when the surface charge density (σ_q) is zero. This minimum arises because for σ_q > 0 V (or σ_q < 0 V) mobile ions enter the channel in order to compensate for the electrostatic charge on the inner walls. This increase in the number of charge carriers increases the conductance.

Figures 1e and 1f show color maps for the cation selectivities (α_C) of the fixed-charge and fixed-potential systems. We define α_C as

$$\alpha_C = \frac{|G_C|}{G} \tag{1}$$

where G_C is the conductance due to the flux of cations. In the case of the fixed-charge system (Figure 1e), we predict, as expected, $\alpha_C = 0.5$ for $\sigma_q = 0$ (nonselective channel), $\alpha_C > 0.5$ for $\sigma_q < 0$ (cation-selective channel) and $\alpha_C < 0.5$ for $\sigma_q > 0$ (anion-selective channel).

We will focus now on the conductance and selectivity of the fixed-potential nanochannels, shown in Figures 1d and 1f, respectively. Comparison between these figures and Figures 1c and 1e show important differences between the transport properties of fixed-charge and fixed-potential nanochannels. Let us first analyze the presence of a conductance maximum as a function of the gate potential observed for $|V_{bias}| > 0.5$ V for the voltage-gated nanochannels. Figure 2a shows the effect of V_{gate} on G, for a fixed bias potential, V_{bias} = 0.8 V. The conductance displays a local maximum at V_{gate} = 0.4 V (*i.e.* $V_{gate} = V_{bias}/2$), which, as we show below, arises from the charge distribution on the channel walls induced by the applied transmembrane potential. It is interesting to note that experimentally asymmetric G vs V_{bias} curves has been reported for nanochannel conductive membranes,[11] although in this case the asymmetry is probably due to the adsorption of chloride anions on the gold surface. We expect that, in the future, the predictions in Figure 2a can be observed by single-channel experiments using weakly interacting anions (e.g., ClO_4^-).

The walls of the channel are held at a fixed potential V_{gate}, thus the surface charge density of the membrane walls depends on the position according to the boundary condition for electrostatics:

$$\sigma_q(r, z) = -\varepsilon\varepsilon_0 \hat{n}\cdot\nabla\psi(r, z) \tag{2}$$

where $\hat{\mathbf{n}}$ is a unit vector normal to the wall and $[r, z]$ is a point at the surface of the membrane. The condition (2) applies both to the inner and outer walls of the channel, but we will focus our discussion on the role of the inner walls, because they have a larger effect on the conductance than the outer walls, and explain the surface charge density distribution of the outer walls in the Supporting Information. Figure 2b shows a plot of the surface charge density of the inner wall, $\sigma_q(z)$, as a function of the position across the membrane, z. The plot shows an approximately linear decrease of σ_q vs z when moving from z = 0 (entrance of lower reservoir) to $z = L$ (entrance of upper reservoir). The channel length is much longer than its radius, so

DOI: 10.1021/acs.jpclett.5b01315
J. Phys. Chem. Lett. 2015, 6, 3534−3539

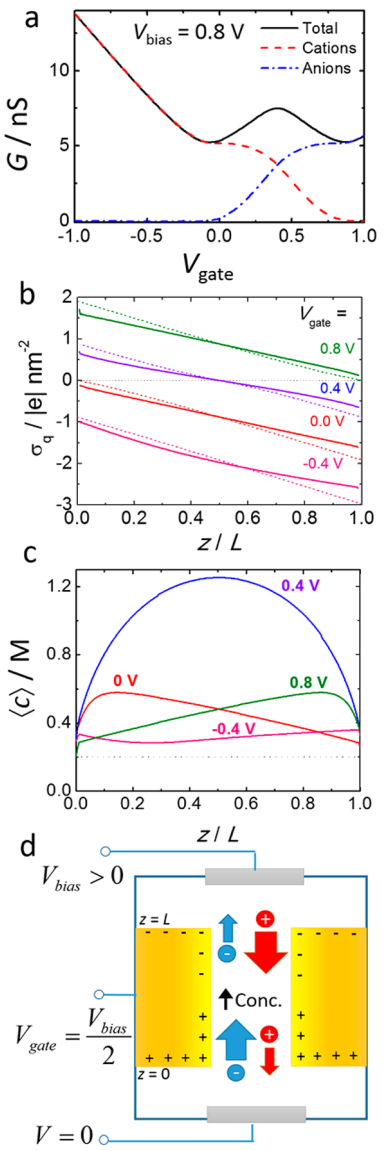

Figure 2. a. Conductance of a fixed-potential nanochannel (L = 250 nm, R = 7.5 nm and a bulk salt concentration of 0.1 M) as a function of the gate potential for a transmembrane bias, V_{bias} = 0.8 V. The plot shows the total conductance (black line), the conductance due to the cations (red dashed line) and the conductance due to the anions (blue dash-dot line). **b.** Surface charge density of the inner nanochannel wall as a function of z, the position across the membrane (z = 0 and L at the mouths of the lower and upper reservoirs, respectively) for the same conditions of panel a. The dashed lines shows the predictions of eqs 3-5 **c.** Radially averaged salt concentration (see eq (6)) as a function of z for the same conditions of panel a. **d.** Schematic representation of the surface charge distribution and ion fluxes for $V_{gate} = V_{bias}/2$ and $V_{bias} > 0$, showing the potential-induced bipolar-diode behavior.

we can assume that the electric field along the axis of the channel is approximately constant (i.e., constant field approximation[22,28]) and that the potential drop in the reservoirs is negligible. Thus, the potential along the channel axis is

$$\psi(r = 0, z) = \frac{z}{L} V_{bias} \tag{3}$$

On the other hand, the potential on the channel wall is fixed to V_{gate}. We can model each slice of the channel at a given z as a cylindrical capacitor with capacitance per unit area C_F,

$$\sigma_q(z) = C_F(V_{gate} - \psi(r = 0, z)) \tag{4}$$

There is no exact analytical solution for C_F for cylindrical channels and the approximate solution based on the linearized Poisson−Boltzmann equation[29] is inaccurate for the present problem. However, in the limit where the channel radius, R, is much larger than the Debye length of the solution (λ_D), C_F approaches its value for planar surfaces,[21] eq 5. In our case, R = 7.5 nm and λ_D = 1 nm, so we expect eq 5 to be a good approximation.

$$\frac{1}{C_F} = \frac{1}{C_{Stern}} + \frac{1}{C_{dl}} = \frac{d_{Stern}}{\varepsilon_{Stern}\varepsilon_0} + \frac{\lambda_D}{\varepsilon_{Sol}\varepsilon_0} \frac{1}{\cosh(\beta|e|(\psi_{Stern} - \psi(r = 0, z))/2)} \tag{5}$$

In eq 5, C_{Stern} and C_{dl} are the contributions from the Stern layer and the double layer to the total capacitance, respectively, d_{Stern} is the thickness of the Stern layer, ε_{Stern} and ε_{Sol} are the relative dielectric constants of the Stern layer and the solution and ψ_{Stern} is the potential at the boundary of the Stern layer and the solution. In the Supporting Information, we explain how to calculate C_F as a function of the position within the channel, z. The combination of eqs 3, 4 and 5 results in predictions (dashed lines in Figure 2b and Figure 3b) that are in very good agreement with the full PNP-NS calculations.

The next question is how the inhomogeneous surface charge distributions shown in Figure 2b dictate the ion conductance and give rise to the conductance maximum at $V_{gate} = V_{bias}/2$ observed in Figure 2a. Figure 2b shows that for $V_{gate} = V_{bias}/2$ = 0.4 V, the lower half of the channel is positively charged and the upper half is negatively charged. This charge distribution corresponds to a bipolar diode,[25,30−33] which exhibits a low-conductance close state and a high-conductance open state, depending on the transmembrane potential. The operation of the fixed-potential nanochannel for $V_{gate} = V_{bias}/2$ is equivalent to the bipolar diode in its open state. The scheme in Figure 2d explains the function of the bipolar diode.[25] The anions (which move toward the positive upper electrode) enter the channel through the positive lower half and exit it through the negative upper half. Thus, due to the electrostatic interactions with the channel walls, the anions experience a small entrance resistance, but they face a large exit resistance. Therefore, the anion concentration in the center of the channel under non-equilibrium conditions increases. The same argument also applies to the cations (inverting the direction of motion), whose concentration also increases in the center of the nanochannel. Therefore, the total concentration of ions inside the channel increases. This result is confirmed by the results in Figure 2c that show an enhancement in the predicted salt concentration averaged over the radial coordinate at the center of the channel ($z = L/2$) and for $V_{gate} = V_{bias}/2$ = 0.4 V. This increase in the total ionic concentration inside the nanochannel gives rise to the conductance maximum observed for $V_{gate} = V_{bias}/2$. As V_{gate} increases or decreases from this value, the bipolar diode effect becomes less effective and thus G decreases. Finally, for very positive or very negative values of V_{gate}, the nanochannel acquires very large positive or negative surface charge densities and, thus, G starts to increase again. In the

DOI: 10.1021/acs.jpclett.5b01315
J. Phys. Chem. Lett. 2015, 6, 3534−3539

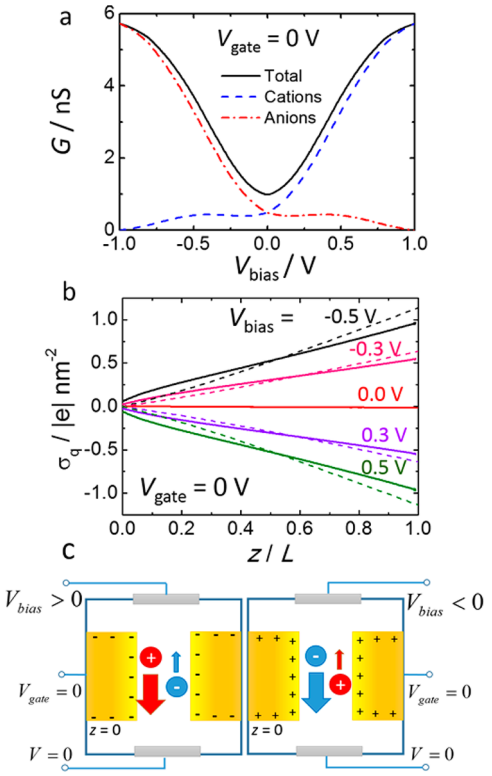

Figure 3. a. Conductance as a function of the transmembrane bias (V_{bias}) for V_{gate} = 0 V. The total, anionic and cationic conductances are shown as solid black lines, dashed-dotted red line and dashed blue lines, respectively. **b**. Surface charge density as a function of z for the same conditions of panel a. The dashed lines show the predictions of eqs 3-5 **c**. Schematic representation of the surface charge distribution and direction of ion fluxes for V_{gate} = 0.

bipolar diode configuration, the charge distribution is symmetric with respect to $z = L/2$ (i.e., $\sigma_q(z) = -\sigma_q(L-z)$); therefore, in this conditions, the channel is completely nonselective, i.e. $\alpha_C = 0.5$ for $V_{gate} = V_{bias}/2$ (see Figure 1f). Note that our system behaves as a bipolar diode only when $V_{gate} = V_{bias}/2$ and, in those conditions, the charge distribution is reversed when the sign of V_{bias} is inverted. Therefore, while the bipolar diode in a fixed-charge channel can operate in open and closed states depending on the sign of the transmembrane bias,[30,32] the potential-induced bipolar diode always operates in the open state (see Figure 1d). It is also interesting to note that we observe the maximum in G vs V_{gate} curves even for wide nanochannels with R = 30 nm (see Figures S6 and S7 in the Supporting Information), which indicates that the potential-induced bipolar diode mechanism holds even when the channel radius is larger than the Debye length of the solution. We ascribe this behavior to the fact that this mechanism, like related concentration polarization effects, is mainly dictated by the ratio of surface to bulk conductivities (known as the Dukhin number) rather that by the ratio between the Debye length and the channel radius.[34]

We analyze next the effect of V_{bias} on the conductance and selectivity, which is negligible for the fixed-charge nanochannels (Figures 1c and 1e), but it is very important for the fixed-potential system (Figures 1d and 1f). Figure 3a shows the total conductance, G, the cation contribution, G_C, and the anion contribution, G_A for $V_{gate} = 0$ as a function of V_{bias}. The conductance depends on the transmembrane bias potential, which indicates a nonohmic behavior (we present examples of I-V curves for the fixed-potential system in the Supporting Information) and shows a minimum for $V_{bias} = 0$, because in this condition $V_{gate} = V_{bias} = 0$ and, thus, $\sigma_q(z) \equiv 0$ according to eq 4. This nonohmic behavior arises because changes in V_{bias} change the surface charge density on the channel walls, which in their turn affects the conductance, G. The effect of V_{bias} on the charge density of the membrane is closely related to bipolar polarization effects.[35]

Figure 3b shows a plot of the charge on the channel surface as a function of the axial position, $\sigma_q(z)$ vs z, for $V_{gate} = 0$ and different values of V_{bias}. Interestingly, inverting the sign of V_{bias} for $V_{gate} = 0$ inverts the polarity of the surface charge and, thus, inverts the selectivity of the channel (see Figure 3a and Figure 1f). This result is in marked contrast with the fixed-charged nanochannel, where the channel is nonselective for $\sigma_Q = 0$ independently of V_{bias} (Figure 1e). For fixed $V_{gate} = 0$, the fixed-potential nanochannel preferentially transports cations for $V_{bias} > 0$ and anions for $V_{bias} < 0$. It is interesting to analyze the direction of the ionic fluxes in these two cases. When $V_{bias} > 0$, the upper electrode is positive and, therefore, anions move upward and cations downward (see scheme in Figure 3c). However, since the channel is cation-selective, there is a preferential downward flux of cations. For $V_{bias} < 0$, the upper electrode is negative, anions move downward and cations upward, but since the channel is anion-selective, there is a preferential downward flux of anions. In other words, for both $V_{bias} > 0$ and $V_{bias} < 0$, there is a net ionic flow toward the lower electrode. This effect has an interesting consequence: if one oscillates V_{bias} between positive and negative values, while holding $V_{gate} = 0$, there is a net flux of neutral salt (i.e., a flux of cations and anions in the same direction and number) toward the lower reservoir. In other words, the proposed configuration pumps neutral salt between reservoirs.

Figure 4a shows a scheme of the proposed salt-pumping experiment: the potentials of the lower electrode and the membrane are set to zero and the potential of upper electrode is oscillated in time. In order to test the salt-pumping mechanism, we performed time-dependent simulations of the PNP-NS equations (the calculations reported so far were steady-state solutions). We started these simulations at $t = 0$ in a steady-state solution of the system at $V_{bias} = V_{osc}$ and evolved them in time while V_{bias} oscillated following a square-wave function with amplitude V_{osc} and frequency ω (see Figure 4b). In Figures 4b-e, we show the results of a simulation for V_{osc} = 0.8 V and ω = 1 kHz. Figure 4c exhibits the cation (J_C) and anion (J_A) fluxes. In our convention, positive fluxes always indicate movement toward the lower electrode. The net flux of neutral salt is given by the total flux of ions toward the lower electrode, $J_T = J_A + J_C$, while the net electric current (i.e., flux of charges) that circulates through the external circuit is $J_{elec} = z_A J_A + z_C J_C = J_C - J_A$. Figure 4d shows the time evolution of J_T and J_{elec}, note that J_T is always positive, which indicates a net and constant flux of salt toward the lower electrode. On the other hand, J_{elec} switches sign with V_{bias}.

Figure 4e shows the time integrals of J_T and J_{elec}:

$$Q_i(t) = \int_0^t J_i(t')dt' \tag{7}$$

where $i = T$ or *elec*. We observe that Q_T (the cumulative flux of salt) increases linearly with time in agreement with a net salt flux toward the lower reservoir. On the other hand, Q_{elec} oscillates around zero. The last result is relevant for applications

DOI: 10.1021/acs.jpclett.5b01315
J. Phys. Chem. Lett. 2015, 6, 3534−3539

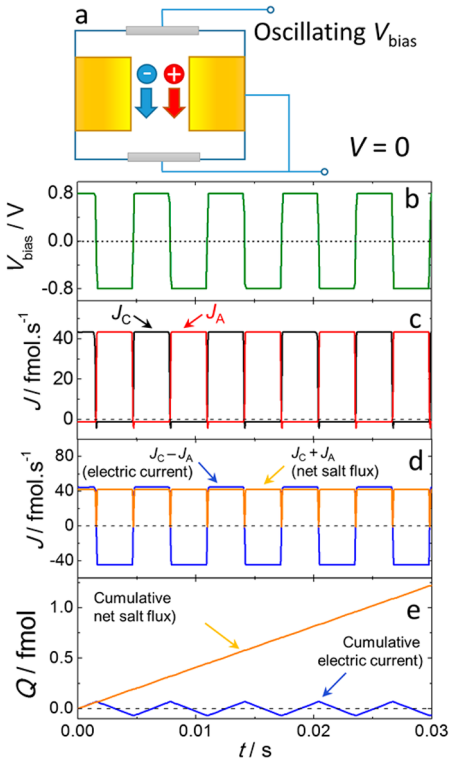

Figure 4. a. The transmembrane potential V_{bias} across a metal membrane containing a nanochannel (L = 250 nm, R = 7.5 nm) is oscillated, while the potential of the membrane is held fixed, V_{gate} = 0 V. **b.** Fluxes of cations and anions as a function of time (in our convention, positive fluxes always correspond to motion to the lower electrode). **c** Electric current, $J_C - J_A$ and net salt flux $J_C + J_A$ as a function of time. **d.** Time integrals of the fluxes in panel c.

in desalinization because ion currents are transformed into electric currents by redox reactions in the reversible electrodes located in the upper and lower reservoirs. The electrodes themselves are reactants in these redox reactions (i.e., Ag and AgCl in an AgCl electrode),[21] hence a net flux of electric charge (i.e., continuous grow of Q_{elec}) would eventually consume the electrodes completely. In the case of Figure 4e, Q_{elec} returns to zero after each cycle of oscillation of V_{bias}, thus the reactants consumed in the first half of the oscillation are regenerated in the second half (this characteristic differentiates our system from single-ion ratchets,[36,37] where a nonzero net electric charge circulates through the external circuit in each oscillation cycle).

In our calculations, the time scale of ion reorganization determines the charge efficiency (CE), which we define as the number of ions that are pumped to the lower electrode per electron that circulates through the external circuit, *i.e.* $CE = \langle J_T \rangle_\tau / \langle |J_{elec}| \rangle_\tau \cdot 100\%$, where $\langle ... \rangle_\tau$ indicates averaging over an oscillation cycle (note that $\langle J_{elec} \rangle_\tau$ is zero, whereas $\langle |J_{elec}| \rangle_\tau$ is different from zero). For low frequencies, the charge efficiency is dictated by the steady-state ion selectivity and, thus, it can be very large: we predict CE = 94% for ω = 1 kHz (calculations in Figure 4). As the frequency increases, ions cannot reach steady-state conditions after each jump of the transmembrane potential (see Supporting Information) and therefore the charge efficiency decreases to CE = 83% for ω = 100 kHz and 5.8% for ω = 10 MHz.

In summary, we presented the first systematic theoretical study of nanochannels in fixed-potential membranes, showed that their conductance properties differ from those of nanochannels in fixed-charge membranes and demonstrated a pump of neutral salt by oscillating the transmembrane potential, which may have potential application for desalinization. In future work, we will provide an in-deep analysis of the efficiencies of salt-separation and energy consumption for the salt-pumping effect.

■ ASSOCIATED CONTENT

Supporting Information

Implementation and numerical solution of the PNP-NS equations, comparison with calculations without electroosmotic effects, surface charge distribution on the outer walls, simple model to calculate the surface charge in fixed-potential nanochannels, $I-V$ curves for fixed-potential nanochannels and the effect of the oscillation frequency on ionic fluxes. The Supporting Information is available free of charge on the ACS Publications website at DOI: 10.1021/acs.jpclett.5b01315.

(PDF)

■ AUTHOR INFORMATION

Corresponding Author

*E-mail: igalsz@northwestern.edu.

Notes

The authors declare no competing financial interest.

■ ACKNOWLEDGMENTS

This work was supported as part of the Center for Bio-Inspired Energy Science, an Energy Frontier Research Center funded by the U.S. Department of Energy, Office of Science, Basic Energy Sciences, under Award no. DE-SC0000989. This research was supported in part through the computational resources and staff contributions provided by the Quest high performance computing facility at Northwestern University, which is jointly supported by the Office of the Provost, the Office for Research, and Northwestern University Information Technology. M.T. is a fellow of CONICET (Argentina).

■ REFERENCES

(1) Tagliazucchi, M.; Szleifer, I. Transport Mechanisms in Nanopores and Nanochannels: Can We Mimic Nature? *Mater. Today* **2015**, *18*, 131−142.

(2) Hou, X.; Zhang, H. C.; Jiang, L. Building Bio-Inspired Artificial Functional Nanochannels: From Symmetric to Asymmetric Modification. *Angew. Chem., Int. Ed.* **2012**, *51*, 5296−5307.

(3) Soler-Illia, G. J. A. A.; Azzaroni, O. Multifunctional Hybrids by Combining Ordered Mesoporous Materials and Macromolecular Building Blocks. *Chem. Soc. Rev.* **2011**, *40*, 1107−1150.

(4) Miller, S. A.; Martin, C. R. Redox Modulation of Electroosmotic Flow in a Carbon Nanotube Membrane. *J. Am. Chem. Soc.* **2004**, *126*, 6226−6227.

(5) Buyukserin, F.; Kohli, P.; Wirtz, M. O.; Martin, C. R. Electroactive Nanotube Membranes and Redox-Gating. *Small* **2007**, *3*, 266−270.

(6) Nishizawa, M.; Menon, V. P.; Martin, C. R. Metal Nanotubule Membranes with Electrochemically Switchable Ion-Transport Selectivity. *Science* **1995**, *268*, 700−705.

(7) Kang, M. S.; Martin, C. R. Investigations of Potential-Dependent Fluxes of Ionic Permeates in Gold Nanotubule Membranes Prepared Via the Template Method. *Langmuir* **2001**, *17*, 2753−2759.

(8) Martin, C. R.; Nishizawa, M.; Jirage, K.; Kang, M. Investigations of the Transport Properties of Gold Nanotubule Membranes. *J. Phys. Chem. B* **2001**, *105*, 1925−1934.

DOI: 10.1021/acs.jpclett.5b01315
J. Phys. Chem. Lett. 2015, 6, 3534−3539

(9) Majumder, M.; Zhan, X.; Andrews, R.; Hinds, B. J. Voltage Gated Carbon Nanotube Membranes. *Langmuir* **2007**, *23*, 8624−8631.
(10) Wu, J.; Zhan, X.; Hinds, B. J. Ionic Rectification by Electrostatically Actuated Tethers on Single Walled Carbon Nanotube Membranes. *Chem. Commun.* **2012**, *48*, 7979−7981.
(11) Gao, P.; Martin, C. R. Voltage Charging Enhances Ionic Conductivity in Gold Nanotube Membranes. *ACS Nano* **2014**, *8*, 8266−8272.
(12) Rutkowska, A.; Freedman, K.; Skalkowska, J.; Kim, M. J.; Edel, J. B.; Albrecht, T. Electrodeposition and Bipolar Effects in Metallized Nanopores and Their Use in the Detection of Insulin. *Anal. Chem.* **2015**, *87*, 2337−2344.
(13) Karnik, R.; Fan, R.; Yue, M.; Li, D.; Yang, P.; Majumdar, A. Electrostatic Control of Ions and Molecules in Nanofluidic Transistors. *Nano Lett.* **2005**, *5*, 943−948.
(14) Liu, Y.; Huber, D. E.; Dutton, R. W. Limiting and Overlimiting Conductance in Field-Effect Gated Nanopores. *Appl. Phys. Lett.* **2010**, *96*, 253108.
(15) Liu, Y.; Huber, D. E.; Tabard-Cossa, V.; Dutton, R. W. Descreening of Field Effect in Electrically Gated Nanopores. *Appl. Phys. Lett.* **2010**, *97*, 143109.
(16) Boon, N.; Olvera de la Cruz, M. 'Soft' Amplifier Circuits Based on Field-Effect Ionic Transistors. *Soft Matter* **2015**, *11*, 4793−4798.
(17) Tagliazucchi, M.; Calvo, E. J.; Szleifer, I. Molecular Theory of Chemically Modified Electrodes by Redox Polyelectrolytes under Equilibrium Conditions: Comparison with Experiment. *J. Phys. Chem. C* **2008**, *112*, 458−471.
(18) Hamelin, A. The Surface State and the Potential of Zero Charge of Gold (100): A Further Assessment. *J. Electroanal. Chem.* **1995**, *386*, 1−10.
(19) Ai, Y.; Zhang, M.; Joo, S. W.; Cheney, M. A.; Qian, S. Effects of Electroosmotic Flow on Ionic Current Rectification in Conical Nanopores. *J. Phys. Chem. C* **2010**, *114*, 3883−3890.
(20) Corry, B.; Kuyucak, S.; Chung, S. H. Tests of Continuum Theories as Models of Ion Channels. II. Poisson-Nernst-Planck Theory Versus Brownian Dynamics. *Biophys. J.* **2000**, *78*, 2364−2381.
(21) Bard, A. J.; Faulkner, L. R. *Electrochemical Methods*, 2nd ed.; John Wiley and Sons: New York, 2001.
(22) Vlassiouk, I.; Smirnov, S.; Siwy, Z. Ionic Selectivity of Single Nanochannels. *Nano Lett.* **2008**, *8*, 1978−1985.
(23) Schoch, R. B.; Han, J.; Renaud, P. Transport Phenomena in Nanofluidics. *Rev. Mod. Phys.* **2008**, *80*, 839−883.
(24) Tagliazucchi, M.; Rabin, Y.; Szleifer, I. Ion Transport and Molecular Organization Are Coupled in Polyelectrolyte Modified Nanopores. *J. Am. Chem. Soc.* **2011**, *133*, 17753−17763.
(25) Daiguji, H. Ion Transport in Nanofluidic Channels. *Chem. Soc. Rev.* **2010**, *39*, 901−911.
(26) Ramírez, P.; Gómez, V.; Cervera, J.; Schiedt, B.; Mafé, S. Ion Transport and Selectivity in Nanopores with Spatially Inhomogeneous Fixed Charge Distributions. *J. Chem. Phys.* **2007**, *126*, 194703.
(27) Stein, D.; Kruithof, M.; Dekker, C. Surface-Charge-Governed Ion Transport in Nanofluidic Channels. *Phys. Rev. Lett.* **2004**, *93*, 035901−1.
(28) Goldman, D. E. Potential, Impedance and Rectification in Membranes. *J. Gen. Physiol.* **1943**, *27*, 37−60.
(29) Rice, C. L.; Whitehead, R. Electrokinetic Flow in a Narrow Cylindrical Capillary. *J. Phys. Chem.* **1965**, *69*, 4017.
(30) Tagliazucchi, M.; Rabin, Y.; Szleifer, I. Transport Rectification in Nanopores with Outer Membranes Modified with Surface Charges and Polyelectrolytes. *ACS Nano* **2013**, *7*, 9085−9097.
(31) Daiguji, H.; Oka, Y.; Shirono, K. Nanofluidic Diode and Bipolar Transistor. *Nano Lett.* **2005**, *5*, 2274−2280.
(32) Vlassiouk, I.; Smirnov, S.; Siwy, Z. Nanofluidic Ionic Diodes. Comparison of Analytical and Numerical Solutions. *ACS Nano* **2008**, *2*, 1589−1602.
(33) Vlassiouk, I.; Siwy, Z. S. Nanofluidic Diode. *Nano Lett.* **2007**, *7*, 552−556.
(34) Zangle, T. A.; Mani, A.; Santiago, J. G. Theory and Experiments of Concentration Polarization and Ion Focusing at Microchannel and Nanochannel Interfaces. *Chem. Soc. Rev.* **2010**, *39*, 1014−1035.
(35) Fosdick, S. E.; Knust, K. N.; Scida, K.; Crooks, R. M. Bipolar Electrochemistry. *Angew. Chem., Int. Ed.* **2013**, *52*, 10438−10456.
(36) Siwy, Z.; Fuliński, A. Fabrication of a Synthetic Nanopore Ion Pump. *Phys. Rev. Lett.* **2002**, *89*, 198103/1−198103/4.
(37) Ramirez, P.; Gomez, V.; Ali, M.; Ensinger, W.; Mafe, S. Net Currents Obtained from Zero-Average Potentials in Single Amphoteric Nanopores. *Electrochem. Commun.* **2013**, *31*, 137−140.

DOI: 10.1021/acs.jpclett.5b01315
J. Phys. Chem. Lett. 2015, 6, 3534−3539